

Electronic Structure and Optical Properties of the Lonsdaleite Phase of Si, Ge and diamond

Amrit De^{1,2} and Craig E. Pryor¹

¹*Department of Physics and Astronomy and Optical Science and Technology Center, University of Iowa, Iowa City, Iowa 52242*

²*Department of Physics and Astronomy, University of California, Riverside, CA 92506*

(Dated: October 30, 2012)

Crystalline semiconductors may exist in different polytypic phases with significantly different electronic and optical properties. In this paper, we calculate the electronic structure and optical properties of diamond, Si and Ge in the lonsdaleite (hexagonal-diamond) phase. We use an empirical pseudopotentials method based on transferable model potentials, including spin-orbit interactions. We obtain band structures, densities of states and complex dielectric functions calculated in the dipole approximation for light polarized perpendicular and parallel to the c -axis of the crystal. We find strong polarization dependent optical anisotropy. Simple analytical expressions are provided for the dispersion relations. We find that in the lonsdaleite phase, diamond and Si remain indirect gap semiconductors while Ge is transformed into a direct gap semiconductor with a significantly smaller band gap.

PACS numbers: 71.15.Dx, 71.20.-b, 78.20.-e, 78.20.Ci

I. INTRODUCTION

It is well known that under extreme conditions a crystalline material may undergo a structural transition to a phase which remains effectively stable upon returning to standard thermodynamic conditions. The existence of such phases, polymorphism in compounds and allotropy in elemental crystals, results in materials with differing electrical and optical properties, such as diamond and graphite. Polytypism is a particular case of polymorphism in which the coordination number does not change. For example, III-V and group-IV semiconductors can crystallize in their non-naturally occurring polytypic phase while maintaining their tetrahedral coordination¹. For example, III-V semiconductors can crystallize in either the zincblende (ZB) phase or the hexagonal wurtzite (WZ) phase. Under extreme conditions cubic diamond (CD) transforms to a hexagonal wurtzite crystal, known as lonsdaleite (LD). The form of diamond was not discovered until 1967 when it was found in a meteorite². It was synthesized soon thereafter³ and is now believed to be the hardest known substance⁷.

The high pressure phases of Si and Ge have been investigated^{1,4} and it has been determined that both undergo a series of structural phase transitions from cubic, to β -Sn, to simple hexagonal, to an orthorhombic phase, to hexagonal closed packed, to a face centered cubic phase^{1,4}. On the other hand, III-V semiconductors typically crystallize either in β -Sn, nickelene (NiAs) or rocksalt structures when subjected to high temperature and pressure^{1,4}. More recently, the growth of WZ phase bulk GaAs was achieved under extreme conditions⁵.

Extreme temperatures and pressure are not the only ways to achieve WZ or LD growth. Laser ablation have been used to synthesize stable LD phase Si⁶. III-V nanowires tend to crystallize in the WZ phase⁷⁻⁹. This has been attributed to various factors such as the

small nanowire radii^{10,11}, growth kinetics¹², interface energies¹³ and electron accumulation at the catalyst's interstitial site¹⁴. It is now believed that the tendency of nanowires to crystallize in WZ/LD phase may be true for group-IV semiconductors as well¹⁵. It has been experimentally found that Si nanowires with a radius in excess of 10 nm tend to crystallize in the LD phase¹⁶ and a number of recent theoretical investigations have confirmed that the hexagonal LD phase is the more stable for Si nanowires exceeding certain critical dimensions¹⁷⁻²⁰. Similar structural phase transitions are expected for Ge nanowires as well¹⁸.

Semiconductor nanowires have attracted much interest due to their potential applications such as photovoltaic cells²¹⁻²³, nano-mechanical resonator arrays²⁴, THz detectors^{25,26}, single photon detectors²⁷⁻²⁹, field-effect transistors^{30,31}, single-electron transistors, and other devices³²⁻³⁷. In addition, the quasi 1-D nature of nanowires allows materials with large lattice mismatches to be combined to form heterostructures that are not possible in planar structures. The design and characterization of such devices requires an understanding of the electronic and optical properties of WZ/LD phase semiconductors. Even though bulk LD phase Si, Ge and diamond have been synthesized in the laboratory, their electronic structure still remains experimentally unverified.

Since these materials may be used for spin based devices, spin-orbit interactions should be included. The band structures and dielectric functions for LD phase diamond, Si and Ge has been calculated using empirical pseudopotentials³⁸, however these calculations were done without the inclusion of spin-orbit interactions. The bandstructure of LD phase diamond Si and Ge have also been calculated using density functional theory³⁹⁻⁴¹, however these methods have well known shortcomings in predicting energies of excited states. Therefore, there is a need for accurate empirically based band structures including spin.

In this paper, we first present bulk electronic band structure calculations for diamond, Si and Ge in the LD phase using empirical pseudopotentials with the inclusion of spin-orbit interactions. These calculations are based on transferable model pseudopotentials assuming an ideal LD structure. The spherically symmetric ionic model potentials are first obtained by fitting the calculated bulk energies of the cubic polytype to experiment. The band structure of the LD polytype is then obtained by transferring the spherically symmetric model pseudopotentials to the LD crystal structure. These model potentials are expected to be transferable between polytypes due to the similarities in their crystal structures. Like the cubic structure, the LD structure is built from tetrahedrons of the same atom but are stacked differently. In both structures all of the nearest neighbors and nine out of the twelve second nearest neighbors are at identical crystallographic locations⁴² and all the second nearest neighbors are equidistant. Hence the local electronic environment should be very similar in both polytypes. This method has proven to be quite successful in obtaining the bulk band structures of various semiconductor polytypes in the past^{38,43–50}. We have used this method to predict the band structures of WZ phase III-V semiconductors⁵¹ and our calculations are in excellent agreement with experiment for the cases for which the WZ band gaps are known (namely GaAs, InP and InAs). Since then, a number of recent experiments have provided further confirmations of the predicted band gaps (and their respective symmetries)^{52–56} and the effective mass of InAs_{WZ} ⁵⁷.

We have also calculated the dielectric functions for diamond, Si and Ge in the LD phase in the linear response regime within the electric dipole approximation for light polarized parallel and perpendicular to the c-axis of the crystal. These calculations are in part motivated by recent experimental results showing that the photoluminescence (PL) intensity in nanowires is strongly polarization dependent^{8,52,58–62}, including Si nanowires⁶³. Nanowire polarization effects can arise from the dielectric mismatch at the wire surface⁵⁸, electron-hole recombination selection rules^{64–66}, as well as from the underlying WZ-type crystal structure^{67–72}. The dominant effect could be more easily identified if the optical dielectric functions for these semiconductors were easily available. However, experimentally measuring optical dielectric functions for LD phase semiconductors is difficult due to the extreme conditions required for growing bulk samples.

Our dielectric function calculations are carried out within the one-particle picture. Much has been done in recent years to include the effects of two particle contributions (such as electron-hole interactions) in the dielectric function^{73–79}. In the case of *first principles* calculations, this improves agreement with experiment for the low energy part of the optical spectrum⁷³. However, the dominant contribution to the dielectric function comes from one-particle calculations, which by itself tend to be in good agreement with experiment^{80–82}. Moreover, while two-particle corrections improve *ab-initio* di-

electric functions⁵⁰, empirical methods include some two-particle effects through their fit to the experimental data (which includes such effects). Typically, dielectric functions calculated using EPMs are in good agreement with experiment⁵⁰.

The required momentum matrix elements, required for our calculations, are obtained from the pseudopotential wave functions. In general, momentum matrix elements for pseudopotential calculations need to be corrected for the missing the core states. Such corrections are typically done using nonlocal terms^{83–86}, which can also account the exchange and correlations effects as well^{87–89}. In our calculations, nonlocal effects are included in the form of spin orbit interactions only.

Another problem with *ab-initio* dielectric function calculations is that ϵ_0 is often overestimated^{90–92}. This is then improved upon by the inclusion of local field effects⁷⁴ such as electron-phonon interactions, which typically affect the low frequency part of the dielectric function (terahertz regime). However, this is not necessary in our case since local field effects shift the peak positions⁷⁵. The EPM includes such effects through the fitting to experiments which necessarily include the effects.

We instead adopt a simpler approach to take the missing core states and local field effects into account. We correct the static dielectric function, ϵ_0 , for the unknown polytype by making use of the *known* ϵ_0 of the cubic phases of diamond, Si and Ge. First, the optical dielectric functions for these cubic group-IV semiconductors are calculated. The optical sum rules are then used to obtain a set of constants which normalizes the calculated cubic ϵ_0 to their respectively known experimental values. Since the constituent element of each polytype is the same, corrections to account for the missing core states should be nearly the same and transferable between polytypes. These normalization constants are then used to correct ϵ_0 for the unknown polytypes (LD), which therefore also corrects the LD phase dielectric functions as well. Unlike calculations involving local field effects, our simple approach fixes ϵ_0 without shifting peak positions.

This paper is organized as follows. Section II outlines the empirical pseudopotential method, followed by a description of both the cubic and hexagonal band structures, and a discussion of the respective symmetries of the two polytypes in section III. Our results are in section IIIB where we present the calculated band structures, densities of states (DOS), effective masses for zone center states and transition energies at various high symmetry points. The optical dielectric functions and reflectivity spectra are given in section IV. Finally, we summarize our results in section V.

II. EMPIRICAL MODEL PSEUDOPOTENTIALS

We use the empirical pseudopotential formalism of Cohen and Chelikowsky⁵⁰. However, rather than discrete form factors we use continuous model potentials so they

are transferable between polytypes. The pseudopotential Hamiltonian consists of the kinetic, local pseudopotential (V_{pp}) and SO interaction (V_{so}) terms,

$$H = \frac{-\hbar^2 \mathbf{K}^2}{2m} + V_{pp} + V_{so}. \quad (1)$$

In a periodic crystal V_{pp} can be expanded in terms of plane waves as

$$V_{pp}(\mathbf{r}) = \frac{1}{N} \sum_{\mathbf{G}, \alpha} \sum_{j=1}^N V_{\alpha}^{FF}(\mathbf{G}) e^{i\mathbf{G} \cdot (\mathbf{r} - \boldsymbol{\tau}_{\alpha,j})} \quad (2)$$

where \mathbf{G} are reciprocal lattice vectors, α labels the atom type, $V_{\alpha}^{FF}(\mathbf{G})$ is the form factor of the α^{th} type of atom, N is the number of atoms per unit cell of a given type, and $\boldsymbol{\tau}_{\alpha,j}$ is the position of atom number j of type α .

For a compound with only one type of atom, the pseudopotential is simply

$$\langle \mathbf{G}' | V_{pp} | \mathbf{G} \rangle = V^{FF}(\mathbf{G}' - \mathbf{G}) S(\mathbf{G}' - \mathbf{G}) \quad (3)$$

where the structure factor is

$$S(\mathbf{G}) = \frac{1}{N} \sum_j \exp(-i\mathbf{G} \cdot \boldsymbol{\tau}_j). \quad (4)$$

V^{FF} can be obtained in various ways^{50,93}. In the empirical pseudopotential approach the atomic form factors are adjusted so the calculated energies at various high symmetry points fit experiment. In order for pseudopotentials to be transferable between polytypes (having different \mathbf{G} 's) $V^{FF}(\mathbf{G})$ should be a continuous function of \mathbf{G} . A wide variety of such model potentials have been used in literature^{46,93-96}, and use potentials of the form

$$V^{FF}(\mathbf{G}) = (x_1 G + x_2) [1 + \exp(x_3 G^2 + x_4)]^{-1} \quad (5)$$

where $G = |\mathbf{G}| \times a/2\pi$, and x_j are adjustable parameters used to fit each material's cubic phase bandstructure to experiment. Model potentials that yield an accurate band structure of a known polytype should reliably predict the band structure for the unknown polytype if the electronic environment in the two crystals structures are similar.

We take spin-orbit coupling into account by including the interaction^{97,98}

$$\begin{aligned} \langle \mathbf{K}', s' | V_{so} | \mathbf{K}, s \rangle &= (\mathbf{K}' \times \mathbf{K}) \cdot \langle s' | \boldsymbol{\sigma} | s \rangle \\ &\sum_l \lambda_l P'_l(\cos \theta_{\mathbf{K}', \mathbf{K}}) S(\mathbf{K}' - \mathbf{K}) \end{aligned} \quad (6)$$

It is not necessary to expand Eq. 6 beyond $l = 2$ since group-IV semiconductors do not have core shells filled beyond d -orbitals. For Ge the terms up to $l = 2$ in Eq. 7 are included, while for Si and diamond we only go up to $l = 1$. Expanding Eq. 6 up to $l = 2$, the spin-orbit coupling term is

$$\begin{aligned} \langle \mathbf{K}', s' | V_{so} | \mathbf{K}, s \rangle &= -i(\hat{\mathbf{K}}' \times \hat{\mathbf{K}}) \cdot \langle s' | \boldsymbol{\sigma} | s \rangle \\ &\left[(\lambda_p + \lambda_d \hat{\mathbf{K}}' \cdot \hat{\mathbf{K}}) S(\mathbf{G}' - \mathbf{G}) \right] \end{aligned} \quad (7)$$

λ_l is a coefficient that can be written in terms of the core wave functions

$$\lambda_l = \mu_l \beta_{nl}(\mathbf{K}') \beta_{nl}(\mathbf{K}) \quad (8)$$

$$\beta_{nl}(K) = C \int_0^\infty i^l \sqrt{4\pi(2l+1)} j_{nl}(Kr) R_{nl}(r) r^2 dr \quad (9)$$

where $\boldsymbol{\sigma}$ s are the Pauli matrices, $\mathbf{K} = \mathbf{G} + \mathbf{k}$, θ is the angle between \mathbf{K} and \mathbf{K}' , and μ_l are adjustable parameters used to fit the spin-orbit splitting energies to experiment⁹⁸. The overlap integral, β_{nl} , is constructed from the radial part of the core wave function, R_{nl} , which is an approximate solution to the Hartree-Fock equations which we obtain from Herman-Skillman tables⁹⁹. C is a normalization constant such that $\beta_{nl}(K)/K$ approaches unity in the limit K goes to zero. Spin-orbit interactions are included for only the outer most p shells ($n = 4$ in Ge, $n = 3$ in Si, and $n = 2$ in diamond) and d shells ($n = 3$ in Ge).

III. BAND STRUCTURES AND CRYSTAL SYMMETRIES

A. Lonsdaleite Crystal Structure and Symmetries

The LD/WZ crystal structure is constructed from two interpenetrating hexagonal close-packed (HCP) lattices, just as the diamond/ZB structure is constructed from two interpenetrating FCC lattices. For ideal crystals, the lonsdaleite lattice constant is related to the diamond lattice constant as $a = a_{cubic}/\sqrt{2}$ and the lattice constant along the c -axis (the [111] direction) is given by $c = \sqrt{1/u} a$. We assume an ideal LD crystal with $u = 3/8$ in this paper, giving $a = 2.522 \text{ \AA}$ and $c = 4.119 \text{ \AA}$ for diamond, both of which are in agreement with the experimental values of $a = 2.52 \text{ \AA}$ and $c = 4.12 \text{ \AA}$ ³. In the case of LD phase Si, a wide range of measured lattice constants have been reported with $(a, c) = (3.84 \text{ \AA}, 6.280 \text{ \AA})$ ⁶, $(3.84 \text{ \AA}, 6.180 \text{ \AA})$ ¹⁰⁰, $(3.837 \text{ \AA}, 6.316 \text{ \AA})$ ¹⁰¹. Assuming an ideal LD crystal structure, we use $a = 3.836 \text{ \AA}$ and $c = 6.264 \text{ \AA}$ for Si. For Ge the ideal lattice constants are $a = 3.993 \text{ \AA}$ and $c = 6.520 \text{ \AA}$, which is within 1 % of the experimental values¹⁰² of $a = 3.96 \text{ \AA}$ and $c = 6.57 \text{ \AA}$.

When viewed along the [111] direction, the inter-layer atomic bonds in LD lie in an eclipsed conformation, defining the axis of hexagonal symmetry while in the CD structure the inter-layer atomic bonds are in a staggered conformation, making all four body diagonals of the cube equivalent. The nearest neighbors are the same in the two polytypes (due to their tetrahedral symmetry), and nine of the twelve next nearest neighbors are in identical positions in both crystals and the remaining three next nearest neighbors are equidistant. These structural similarities suggests that the local electronic environment will

be very similar in the two crystals, and hence the atomic form factors should be nearly identical in both polytypes.

The LD crystal structure has a space group symmetry classification of D_{6h}^4 (or $P6_3/mmc$). It has inversion symmetry in addition to all the symmetries of WZ. The irreducible representation of the space group of Γ are just the representations of the point group D_{6h} (which has all the symmetries of C_{6v} as well as inversion symmetry). While moving along the k_z direction the symmetry is lowered to C_{6v} . The A , K and H all have point group symmetries of D_{3h}^{103} . D_{3h} is isomorphic to C_{6v} and is a symmorphic invariant subgroup of D_{6h} . The L and M points have D_{2h} symmetry. The point group operations must be followed by appropriate translations in order to obtain the irreducible representations of the wave functions at the high symmetry points. For example at the Γ point the point group operations must be followed by a translation $\tau = (0, 0, c/2)$.

The LD crystal structure has lower symmetry than the cubic diamond structure, and the SO interaction leads to additional lifting of orbital degeneracies. In the absence of spin-orbit coupling, the hexagonal crystal field of LD splits the p -like Γ_{15} state of cubic structure into a four-fold degenerate Γ_6 and a doubly degenerate Γ_1 . In terms of the p -orbitals, these states are $p_z \rightarrow \Gamma_1$ are $p_x, p_y \rightarrow \Gamma_6$. With the inclusion of spin-orbit coupling, Γ_{6v} splits into the Γ_{9v} heavy-hole and the Γ_{7v} light-hole. Therefore, all zone center states in LD belong to either Γ_7 , Γ_8 , or Γ_9 with either even or odd parity since LD has a center of inversion. Unlike WZ, there are no spin splittings in LD due to its inversion symmetry.

B. Predicted Lonsdaleite Band Structures

We use spherically symmetric local form factors fit to the CD band structure, which are then transferred to the LD crystal. The potentials should be transferable since the local electronic environments of the two polytypes are very similar. The lonsdaleite primitive unit cell has four atoms. We choose the origin, so that the atoms are located at $\mathbf{v}_1 = \frac{1}{3}\mathbf{a}_1 + \frac{2}{3}\mathbf{a}_2$, $\mathbf{v}_2 = \frac{2}{3}\mathbf{a}_1 + \frac{1}{3}\mathbf{a}_2 + \frac{1}{2}\mathbf{a}_3$, $\mathbf{v}_3 = \mathbf{v}_1 + u\mathbf{a}_3$ and $\mathbf{v}_4 = \mathbf{v}_3 + u\mathbf{a}_3$. Where $\mathbf{a}_1 = (1, 0, 0)a$, $\mathbf{a}_2 = (-1, \sqrt{3}, 0)a/2$ and $\mathbf{a}_3 = (0, 0, c)$ are the primitive lattice vectors. Substituting these atomic positions into Eq. 4, we obtain the following structure factor

$$S = \frac{1}{2} \exp\left(-\frac{iG_y a}{\sqrt{3}} - \frac{iG_z u c}{2}\right) \cos\left(\frac{G_z u c}{2}\right) \times \left[1 + \exp\left(-\frac{iG_x a}{2} + \frac{iG_y a}{2\sqrt{3}} - \frac{iG_z c}{2}\right)\right] \quad (10)$$

where, G_j ($j = x, y, z$) are the components of the reciprocal lattice vector \mathbf{G} .

The calculated band structure and the corresponding density of states (DOS) for diamond, Si and Ge in LD phase are shown in Figs. 1-3. The electronic band structures are calculated in the irreducible wedge of the Brillouin zone. The LD band structure is more complicated

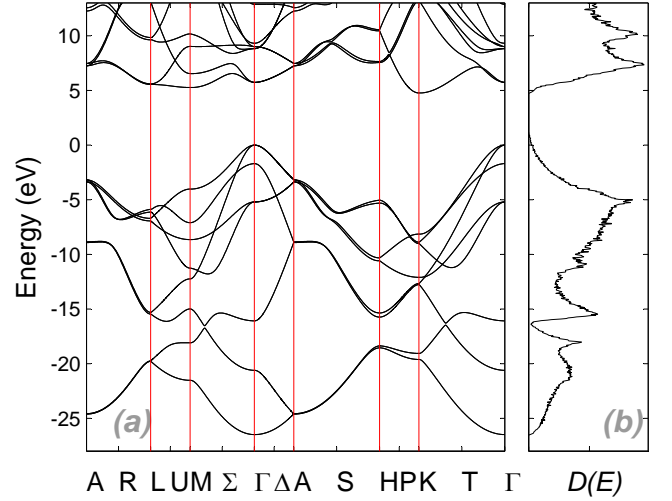


Figure 1. (a) Band structure for diamond in the lonsdaleite phase (b) Density of states.

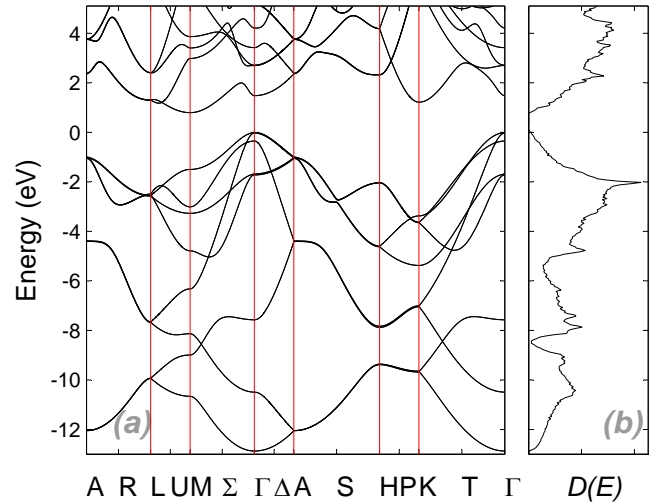


Figure 2. (a) Band structure for Si in the lonsdaleite phase. (b) Density of states.

its CD counter part due to its lower crystal symmetry. For a given energy range, there are roughly twice as many bands for the LD phase. The points, A and H , are special points where the energy levels stick together because the structure factor is zero there.

Due to the similarities of the two crystals, many of the high symmetry points in the Brillouin zones of cubic and LD have a one-to-one correspondence with each other (just as in the case of ZB and WZ). This one to one correspondence is particularly useful in interpreting their respective band structures.

The volume of LD's first Brillouin zone is about half of that of its cubic counter part. Therefore, if one were to take an intersection of the two Brillouin zones such that each of their Γ -points coincide, then the L -point in the cubic structure also coincides with the Γ -point in LD⁴⁰.

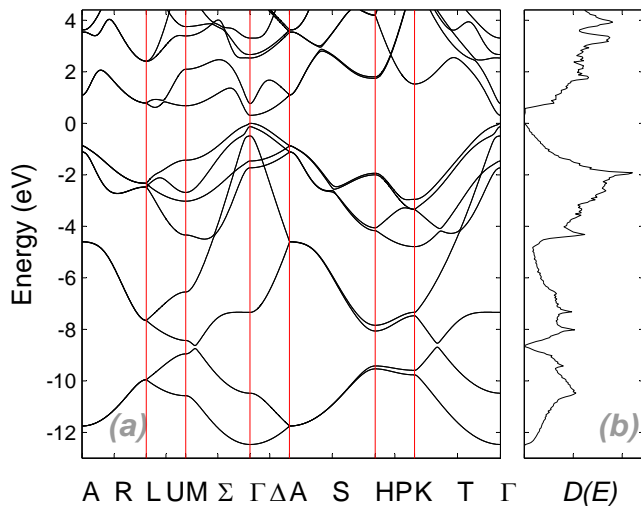


Figure 3. (a) Band structure for Ge in the lonsdaleite phase. (b) Density of states.

Thus, in the free electron model, the zone center LD/WZ energies can be directly predicted from the cubic Γ and L point energies. In single group notation (absence of SO interactions), the cubic Γ_1 , L_1 and L_3 states correspond to Γ_1 , Γ_3 and Γ_5 respectively in LD. However, the presence of the crystal potential will perturb the exact one to one correspondence of the high symmetry point energies. Because of this zone folding of the L -valley, indirect gap cubic materials with an L valley conduction band minima could be expected to have a direct gap in the LD phase (unless the energy of that state was significantly shifted by the crystal potential).

There also are similar correspondences between the high symmetry directions of the two crystals. The $\Lambda(\Gamma \rightarrow L)$ line in the cubic structure corresponds to the $\Delta(\Gamma \rightarrow A)$ line in the LD⁴² structure. Note that there are eight equivalent L directions in the cubic structure. Only the ones that are along the c -axis map on to the Γ_{hex} point. The other six along with X_{cub} maps on to a point on the U_{hex} -line, two thirds away from the M_{hex} point. We label this point as M'_{hex} . The Δ_{cub} line maps onto a line joining M'_{hex} and Γ_{hex} . The Δ_{cub} line is especially important as the band gap for both diamond and Si lies along this line close to X_{cub} .

We list the energies at various high symmetry points along with the corresponding irreducible representations of these states in tables I-III. The irreducible representations of the zone center states was determined by transforming the pseudo wave functions under the symmetry operations of the respective crystallographic point group. The zone center (Γ point) effective masses for diamond, Si and Ge for \mathbf{k} parallel and perpendicular to the c -axis is shown in table IV.

From the band structure calculations, it is seen that in the LD phase, diamond and Si are indirect gap semiconductors. Diamond has a band gap of about 4.767 eV

with band minima occurring at the K -valley. This is in agreement with earlier results obtained by Salehpour and Sathpathy³⁹ where the band minima was also shown to occur at K . Their estimated band gap from LDA calculations (with corrections) was about 4.5 eV. The LD band gap for diamond is also significantly smaller than its cubic phase band gap of 5.4 eV.

In the case of the LD phase Si, the calculated band gap is 0.796 eV and the band minima is at the M -valley. The LD phase gap for Si is a lot smaller than its cubic band gap of about 1.1 eV. In our calculations, Ge is the only direct gap group-IV semiconductor in the LD phase. It has a Γ_8 conduction band minima. The Γ_8 symmetry is due to the fact that cubic phase Ge has a conduction band minima at the L valley, which folds over to Γ_8 in the hexagonal phase.

With the inclusion of SO interactions for LD, the top three valence states are typically (in order of decreasing energy) Γ_9 , Γ_7 , Γ_7 (normal ordering)^{64,104} or Γ_7 , Γ_9 , Γ_7 (anomalous ordering) which results from a negative spin-orbit energy. In our calculations, the top three valence band states in Si and Ge have normal ordering in LD phase, while the top valence band states in diamond have neither normal nor anomalous ordering. Instead the top two valence band states for LD-diamond are Γ_9^- and Γ_8^- . The Γ_7^+ , Γ_7^+ , Γ_9^+ states lie further bellow.

The spin-orbit splitting energy, Δ_{so} and the crystal field splitting, Δ_{cr} , can be extracted using the quasi cubic approximation which assumes the WZ/LD structure to be equivalent to a [111]-strained zincblende structure¹⁰⁵. Δ_{so} and Δ_{cr} are related to the Γ_{7v}^1 light hole and Γ_{7v}^2 light hole energies by

$$E(\Gamma_{7v}^{1,2}) - E(\Gamma_{9v}) = -\frac{\Delta_{so} + \Delta_{cr}}{2} \pm \frac{1}{2} \left((\Delta_{so} + \Delta_{cr})^2 - \frac{\Delta_{so}\Delta_{cr}}{u} \right)^{\frac{1}{2}} \quad (11)$$

where $\sqrt{u} = a/c$ is 3/8 for an ideal WZ/LD structure assumed here. The band ordering and irreducible representations of the zone center states need to be identified before using this equation. We have compiled a shorter table (table-V) for the LD phase semiconductors, that lists the band gap, Δ_{so} , Δ_{cr} , and the offset between the valence band edges of each polytypes.

IV. OPTICAL PROPERTIES

A. Calculations

At normal incidence, for any given polarization, the reflectivity acquires the simple form $R = |(1 - n_i)/(1 + n_i)|^2$, where, n_i ($i = x, y$ or z depending on the surface normal) is the complex index of refraction. In the linear response regime, $n(\omega) = \sqrt{\epsilon(\omega)}$ and the complex dielectric function can be separated into real

IR	E (eV)	IR	E (eV)	IR	E (eV)	IR	E (eV)	IR	E (eV)	IR	E (eV)
Γ_7^+	-26.4861	A_7	-24.6126	L_5	-19.7797	M_5	-21.5188	H_7	-18.5436	K_7	-19.6131
Γ_8^-	-20.6056	A_8	-24.5697	L_5	-19.73	M_5	-18.0857	H_8	-18.3647	K_8	-19.0582
Γ_8^-	-16.081	A_8	-8.9149	L_5	-15.4592	M_5	-14.9875	H_8	-15.7359	K_8	-12.7624
Γ_8^+	-5.2053	A_7	-8.8447	L_5	-15.313	M_5	-12.2387	H_8	-15.3608	K_8	-12.6617
Γ_9^+	-5.1929	A_8	-3.3676	L_5	-6.9353	M_5	-11.2565	H_9	-10.5802	K_9	-12.0976
Γ_7^+	-1.6965	A_9	-3.3601	L_5	-6.6979	M_5	-8.6464	H_7	-10.3175	K_8	-9.0102
Γ_7^-	-0.003	A_9	-3.1847	L_5	-6.1246	M_5	-7.101	H_8	-5.303	K_9	-8.8838
Γ_9^-	0	A_7	-3.1772	L_5	-5.8708	M_5	-4.0212	H_9	-5.03	K_7	-8.1377
Γ_7^-	5.7365	A_7	7.2555	L_5	5.5528	M_5	5.2688	H_9	7.5599	K_9	4.7676
Γ_9^-	5.741	A_9	7.2574	L_5	5.6029	M_5	6.5429	H_7	7.6419	K_7	13.1856
Γ_7^-	8.8245	A_8	7.4665	L_5	9.6269	M_5	9.0309	H_9	10.4545	K_9	13.4011
Γ_9^-	8.8246	A_9	7.4685	L_5	9.8392	M_5	10.1738	H_7	10.5574	K_7	14.0873
Γ_9^+	9.0085	A_7	12.2676	L_5	13.1219	M_5	18.184	H_9	17.4962	K_9	17.121
Γ_8^+	9.0095	A_8	12.5631	L_5	13.3848	M_5	18.2476	H_8	17.5338	K_8	17.5896
Γ_7^+	9.3188	A_7	15.361	L_5	24.929	M_5	20.3734	H_9	19.3015	K_9	18.8105

Table I. Transition energies at various high symmetry points and the respective irreducible representations(IR) for the lonsdaleite phase of diamond. Note that the conduction band minima is in near vicinity of the K valley

IR	E (eV)	IR	E (eV)	IR	E (eV)	IR	E (eV)	IR	E (eV)	IR	E (eV)
Γ_7^+	-12.8713	A_7	-12.0498	L_5	-9.9375	M_5	-10.6599	H_7	-9.3824	K_7	-9.6803
Γ_8^-	-10.4924	A_8	-12.0433	L_5	-9.9237	M_5	-8.992	H_8	-9.3576	K_8	-9.643
Γ_8^-	-7.5715	A_8	-4.406	L_5	-7.6756	M_5	-8.1319	H_8	-7.8786	K_8	-7.0424
Γ_8^+	-1.7207	A_7	-4.3857	L_5	-7.6573	M_5	-6.321	H_7	-7.8319	K_7	-7.0031
Γ_9^+	-1.6793	A_7	-1.0552	L_5	-2.5751	M_5	-4.7847	H_9	-4.6241	K_9	-5.3748
Γ_7^+	-0.3496	A_9	-1.0322	L_5	-2.5516	M_5	-3.2709	H_7	-4.5975	K_8	-3.6509
Γ_7^-	-0.0279	A_8	-1.0192	L_5	-2.5085	M_5	-3.01	H_8	-2.0413	K_9	-3.6304
Γ_9^-	0	A_9	-0.9962	L_5	-2.4906	M_5	-1.4971	H_9	-2.0303	K_7	-3.3739
Γ_8^-	1.4814	A_8	2.3662	L_5	1.2958	M_5	0.7957	H_9	2.3229	K_8	1.2191
Γ_9^-	2.6962	A_7	2.3878	L_5	1.3036	M_5	2.9848	H_8	2.3319	K_9	5.7005
Γ_9^-	2.7151	A_8	3.7479	L_5	2.4036	M_5	3.4078	H_9	4.1826	K_9	6.4501
Γ_7^+	3.4206	A_9	3.7614	L_5	2.4125	M_5	3.8669	H_8	4.1891	K_9	6.475
Γ_7^+	4.2135	A_7	3.7624	L_5	6.695	M_5	5.8173	H_9	6.8291	K_7	6.8974
Γ_9^+	5.1671	A_9	3.7759	L_5	6.705	M_5	7.2281	H_8	6.8401	K_7	6.919
Γ_8^+	5.1779	A_8	7.7044	L_5	9.1484	M_5	7.6228	H_7	7.3607	K_8	6.9399

Table II. Transition energies at various high symmetry points and the respective irreducible representations(IR) for the lonsdaleite phase of Si. Note that the conduction band minima is very close to the M valley

IR	E (eV)	IR	E (eV)	IR	E (eV)	IR	E (eV)	IR	E (eV)	IR	E (eV)
Γ_7^+	-12.4692	A_7	-11.7515	L_5	-9.9534	M_5	-10.5753	H_7	-9.5329	K_7	-9.7671
Γ_8^-	-10.4783	A_8	-11.751	L_5	-9.9492	M_5	-8.9518	H_8	-9.4188	K_8	-9.5896
Γ_8^-	-7.3386	A_8	-4.6049	L_5	-7.6576	M_5	-8.431	H_8	-8.0632	K_8	-7.471
Γ_9^+	-1.7267	A_7	-4.5941	L_5	-7.6503	M_5	-6.548	H_7	-7.8404	K_7	-7.3368
Γ_8^+	-1.4617	A_9	-1.1146	L_5	-2.4754	M_5	-4.3358	H_7	-4.1686	K_8	-4.787
Γ_7^+	-0.4896	A_8	-1.1069	L_5	-2.4673	M_5	-3.023	H_9	-4.0578	K_9	-3.3445
Γ_7^-	-0.1293	A_7	-0.8801	L_5	-2.3285	M_5	-2.6832	H_9	-1.9988	K_7	-3.3327
Γ_9^-	0	A_9	-0.8723	L_5	-2.3199	M_5	-1.4302	H_8	-1.9369	K_9	-2.951
Γ_8^-	0.3103	A_8	1.0951	L_5	0.7849	M_5	0.6828	H_7	1.7489	K_8	1.5267
Γ_7^+	0.7659	A_7	1.1023	L_5	0.7877	M_5	2.0997	H_9	1.8076	K_7	5.5903
Γ_7^+	2.5368	A_7	3.538	L_5	2.4102	M_5	3.3933	H_8	4.1879	K_9	5.6603
Γ_9^-	2.6714	A_9	3.5433	L_5	2.4151	M_5	3.7561	H_7	4.2033	K_7	5.6979
Γ_7^+	3.3102	A_7	3.6279	L_5	6.3148	M_5	5.0137	H_7	6.5626	K_7	5.7016
Γ_8^-	4.7797	A_9	3.6332	L_5	6.3199	M_5	6.6232	H_7	6.6076	K_7	5.7153
Γ_9^+	4.8536	A_7	6.0862	L_5	8.3515	M_5	6.947	H_9	6.6965	K_8	6.4529

Table III. Transition energies at various high symmetry points and the respective irreducible representations(IR) for the lonsdaleite phase of Ge. This is a direct gap semiconductor with a band gap of 0.310 eV.

diamond		Si		Ge	
$m_{ }$	m_{\perp}	$m_{ }$	m_{\perp}	$m_{ }$	m_{\perp}
1.1376	1.1947	1.1365	1.1522	1.1887	1.1988
0.1915	1.1724	0.2697	1.1129	0.3375	1.1500
0.1482	1.8260	0.184	2.4867	0.2153	11.7707
1.1656	0.3104	1.3479	0.1843	1.347	0.1550
1.1697	0.3425	1.3598	0.1916	1.4218	0.1404
0.1810	0.6821	0.1028	0.7687	0.0587	0.3416
0.3414	0.2437	0.5481	0.201	0.1484	0.0871
0.3418	0.3226	0.5637	0.2128	0.6035	0.0672
0.7860	0.3785	1.0483	0.1224	1.0563	0.0852
0.7877	0.3588	0.6496	1.096	0.0516	0.0410
0.2504	0.9981	0.6548	0.9096	0.6213	1.0951
0.2504	2.6106	0.1527	1.0882	0.6604	1.5539
0.9974	0.5130	4.0888	0.1375	4.5651	0.4412

Table IV. Zone center effective masses, parallel and perpendicular to the c axis, for diamond, Si and Ge.

	E_g (eV)	Δ_{so} (eV)	Δ_{cr} (eV)	ΔE_{VB} (eV)
diamond	4.7672 (K_9)	0.0045	1.6950	0.0286
Si	0.7957 (M_5)	0.044	0.3336	-0.1484
Ge	0.310 (Γ_8)	0.404	0.1730	-0.1454

Table V. Energies of the lonsdaleite phase of diamond, Si and Ge. The symmetry of the conduction band minimum is indicated in parenthesis along with the band gap. Δ_{so} and Δ_{cr} are the spin-orbit splitting and crystal-field splitting energies extracted using Eq. (11). $\Delta E_{VB} = E_{VB}^{cubic} - E_{VB}^{LD}$, is the energy difference between the top of the valance bands for the two polytypes.

and imaginary parts $\epsilon(\omega) = \epsilon'(\omega) + i\epsilon''(\omega)$, which are related to each other by the Kramers-Kronig relations.

All dielectric function calculations in this paper are carried out in the long wavelength limit, (*i.e.* assuming only direct band-to-band transitions (same k). We obtain $\epsilon''(\omega)$ using our empirical pseudopotential wave functions. In the electric dipole approximation, the direct transition between an initial state, I , and a final state, J , $\epsilon''(\omega)$ is given by

$$\epsilon''(\omega) = \left(\frac{\hbar\pi^2 e^2}{m^2 \omega^2} \right) \times \sum_{ij} \int_{BZ} |M_{IJ}|^2 \delta(E_{c,j}(\mathbf{k}) - E_{v,i}(\mathbf{k}) - \hbar\omega) d^3k \quad (12)$$

where \int_{BZ} is an integration over the entire Brillouin zone (BZ), \sum_{ij} is a sum over all initial valance band and final conduction band states, and $E_v(\mathbf{k})$ and $E_c(\mathbf{k})$ are the valance and conduction band energies at their respective ks. The delta function is approximated by

$$\delta(\Delta E - \hbar\omega) \approx 2(1 + \cosh[\gamma(\Delta E - \hbar\omega)])^{-1} \quad (13)$$

where γ is an adjustable damping parameter that can be used to phenomenologically incorporate lifetime broadening effects. We used $\gamma = 100 \text{ eV}^{-1}$ which gives a transition linewidth of about 35 meV^{106} .

The real part of the dielectric function, $\epsilon'(\omega)$ is then obtained using the Kramers-Kronig relations

$$\epsilon'(\omega) = 1 + \frac{2}{\pi} \mathcal{P} \int_0^\infty \frac{\omega' \epsilon''(\omega')}{\omega'^2 - \omega^2} d\omega' \quad (14)$$

where \mathcal{P} is the Cauchy principle value.

The momentum matrix elements, for band to band transitions, between the initial state I and and final state J is given by

$$M_{IJ}(\mathbf{k}) = \langle \phi_{I,\mathbf{k}} | \hat{p} | \phi_{J,\mathbf{k}} \rangle \quad (15)$$

where, \hat{p} is the momentum operator. We calculate M_{IJ} using the pseudopotential wave functions, which can be written as

$$\phi_{I,\mathbf{k}}(\mathbf{r}) = \sum_{\mathbf{G}} c_I(\mathbf{k}, \mathbf{G}) \exp[i(\mathbf{k} + \mathbf{G}) \cdot \mathbf{r}] \quad (16)$$

where, $c_I(\mathbf{k}, \mathbf{G})$ are the eigenvector coefficients, for the I^{th} state, obtained by diagonalizing the pseudopotential Hamiltonian at a given wavevector \mathbf{k} . Using Eq.16, M_{IJ} can therefore be rewritten in terms of the expansion coefficients as follows,

$$M_{IJ}(\mathbf{k}) = i \sum_{\mathbf{G}} c_I^*(\mathbf{k}, \mathbf{G}) c_J(\mathbf{k}, \mathbf{G}) [(\mathbf{k} + \mathbf{G}) \cdot \hat{\mathbf{e}}] \quad (17)$$

where, $\hat{\mathbf{e}}$ is the polarization vector. The frequency dependent imaginary part of the dielectric function, $\epsilon''(\omega)$, is then be calculated using Eq.17, for light polarized parallel and perpendicular to the c -axis. In order to evaluate the Brillouin zone integral in Eq.12, we have used a set of 4.5×10^4 special k points. These special k points are generated using the scheme of Monkhorst and Pack¹⁰⁷

The momentum matrix elements calculated using the pseudopotential wave functions need to be corrected for the missing core states⁹³. One way to do this is to include the commutator of the nonlocal pseudopotential and the position operator^{108,109}, while other proposed methods involve the inclusion of a core repair term⁸³. However it should be noted that both techniques cause small changes to the dielectric function (typically less than 5%). Some first principles calculations have even shown that there is almost no difference between dielectric functions calculated using *ab initio* pseudopotential wave functions and those calculated using true electron wave functions⁸⁶.

Our efforts to calculate the dielectric functions of the LD phase of group-IV semiconductors however greatly aided by the fact that the cubic phase dielectric functions of diamond, Si and Ge are already well known. We take advantage of the fact that the pseudopotentials are being transferred between polytypes. Due to the similarity of the electronic environment around an atom in the two polytypes, corrections to account for the missing core states should be nearly the same and transferable between polytypes. This method also accounts for local field effects and static screening effects.

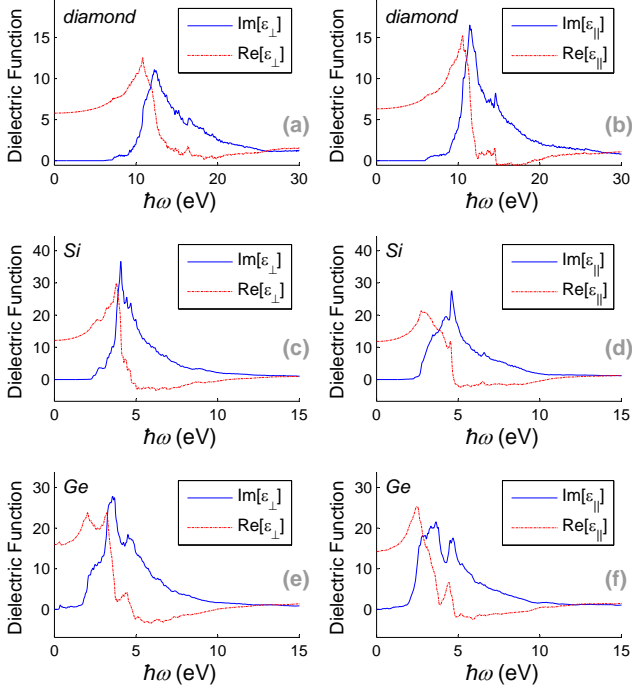


Figure 4. Real and imaginary parts of the complex dielectric function as a function of optical frequency shown here for light polarized (a) E_{\perp} in lonsdaleite phase diamond, (b) E_{\parallel} in lonsdaleite phase diamond, (c) E_{\perp} in lonsdaleite phase Si, (d) E_{\parallel} in lonsdaleite phase Si, (e) E_{\perp} in lonsdaleite phase Ge and (f) E_{\parallel} in lonsdaleite phase Ge

the corresponding reflectivity spectra for both polarizations shows several peaks which originate from interband transitions along various high symmetry points. Each of these crystals have distinct spectral features depend on the details of their electronic structure. For Ge and Si the most prominent features are typically seen up to about 4 eV, whereas for diamond the most prominent peak is seen at about 12 eV. All the group-IV LD phase semiconductors are optically anisotropic as expected. However, diamond exhibits greater optical anisotropy than Si or Ge as seen in the reflectivity spectra (Fig.5). Notice that around 12 eV, the absorption is significantly more for E_{\perp} due the much smaller ϵ_{\perp} structures at the same frequency.

In order to elucidate the the dielectric function's variations about the fundamental absorption edge (FAE), we fit the numerically calculated ϵ_{\perp} and ϵ_{\parallel} , below the Reststrahlen band, to a classical Lorentz oscillator, whose real and imaginary parts are

$$\epsilon'(\omega) = 1 - f \sum_{j=1}^2 \frac{\omega^2 - \Omega_j^2}{(\omega^2 - \Omega_j^2)^2 + (\Gamma_j \omega)^2} \quad (19)$$

$$\epsilon''(\omega) = f \sum_{j=1}^2 \frac{\Gamma_j \omega}{(\omega^2 - \Omega_j^2)^2 + (\Gamma_j \omega)^2} \quad (20)$$

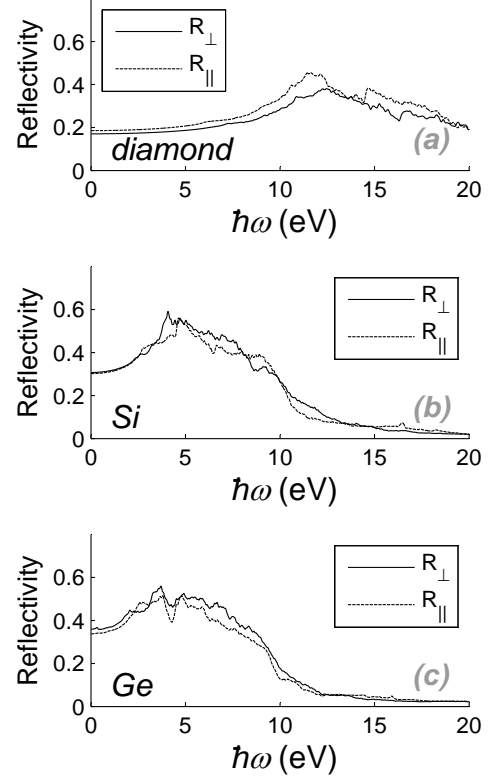


Figure 5. Calculated reflectivity spectra at normal incidence for the lonsdaleite phase of (a) diamond, (b) Si and (c) Ge

Material	ϵ_0^{\perp}	ϵ_0^{\parallel}
diamond	5.7988	6.3192
Si	12.1808	11.8518
Ge	16.0066	14.2896

Table VII. Calculated static dielectric constant for light polarized parallel and perpendicular to the c -axis, for the three lonsdaleite phase group IV semiconductors.

Here, f , Ω_j and Γ_j were used as fitting parameters and are listed in Table VI. Typically, f represents the oscillator strength, Γ_j the relaxation rate and Ω_j is a resonance frequency term.

These fits in terms of the Lorentz oscillators provides an analytical expression for the dielectric function's dispersion relations over the spectral region where there are no discontinuities. Therefore these dispersion relations are valid only within a certain cut-off frequency (ω_K) as listed in Table VI). The fitting parameters, such as f s, Γ_i s and Ω_i s, depend on ω_K and do not necessarily represent trends in the optical properties of these semiconductors. These analytic dispersion relations could be useful for modeling optical devices and multi-layer thin-film structures.

The static dielectric constants were calculated from the imaginary part of the dielectric functions

($\epsilon_o = 1 + 2 \int_0^\infty \epsilon''(\omega) d\omega / \pi\omega$), for light polarized parallel and perpendicular to the c axis, and are listed in Table VII. In general, the semiconductor with the higher atomic number (Z) has the larger static dielectric constant. We also see that $\epsilon_o^\perp < \epsilon_o^\parallel$ in the case of diamond (which has a Γ_7 direct gap), whereas $\epsilon_o^\perp > \epsilon_o^\parallel$ for Si and Ge (which have Γ_8 direct gaps).

A simple explanation for this can be provided based on the optical selection rules. For a given material, ϵ_o depends on the number of allowed transitions and the oscillator strength of each transition. The closer the bands are, the stronger the dipole transitions will be. Consider a small region of ω around the direct band gap where the transitions are the strongest for zone center states. For E_\perp a transition between the Γ_9 heavy-hole (HH) and the Γ_7 (or Γ_8) conduction band is allowed. All three materials Si, Ge and diamond will be optically active. Whereas for E_\parallel the $\Gamma_7^{(1,2)}$ light-hole/split-off hole to Γ_7 conduction band is only allowed for diamond. Si and Ge are completely optically dark in this case. Hence for E_\parallel , diamond has more allowed transitions than for E_\perp (assuming similar oscillator strengths) and therefore its $\epsilon_o^\perp < \epsilon_o^\parallel$. Whereas the opposite is true for Si and Ge.

V. SUMMARY

We have calculated the electronic band structures and dielectric functions for diamond, Si and Ge in lonsdaleite phase using transferable model potentials, including spin-orbit coupling. The potentials should be accurate since the local electronic environment for the cubic and lonsdaleite polytypes are very similar. It is seen that while diamond and Si remain indirect in the lonsdaleite phase, Ge is transformed into a narrow direct-gap semiconductor due to zone folding effects. Hence LD-type Ge will be optically active, which could make it extremely useful for technological applications. We have also tabulated a number of parameters such as high symmetry point energies, their irreducible representations and effective masses, which could be useful for constructing $k \cdot p$ type models. We calculated the frequency dependent complex dielectric functions up to 20 eV for light polarized parallel and perpendicular to the c -axis in the dipole approximation. We find strong optical anisotropy, making LD phase materials potentially useful as nonlinear crystals since their optical birefringence enables them to satisfy phase matching conditions.

VI. APPENDIX

In this appendix we provide the details for our band-structure calculations for the cubic phase of diamond, Si and Ge. The form factors of the cubic polytypes are required for obtaining the bandstructures of the hexagonal

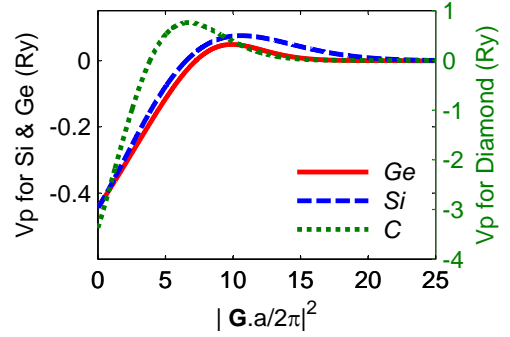


Figure 6. Local atomic form factors (V_p) for diamond (C), Si and Ge. Note that the y-axis for diamond is on the right.

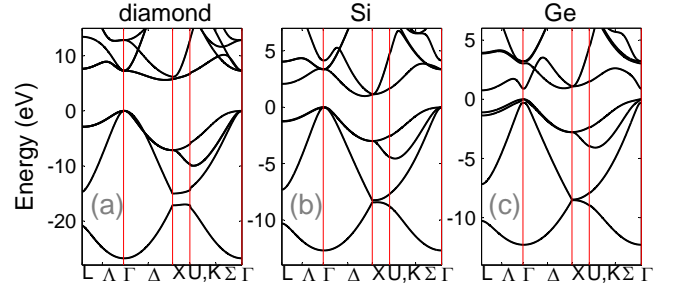


Figure 7. Calculated band structures, with the inclusion of spin-orbit interactions, for the cubic phase of (a) diamond (b) Si and (c) Ge

polytypes. The Hamiltonian, given in Eq.1, is diagonalized with a plane wave basis cutoff of $|\mathbf{G}| \leq 64\pi/a$. As a starting point, our continuous form factors for Si and Ge were first fit to the discrete form factors of Ref.[98] and for diamond, they were fit to the discrete form factors of Ref.[114]. The adjustable parameters x_i , and μ_l in Eqs. 5 and 8 were then adjusted to fit the calculated band structure to the experimental energies of the band extrema of the cubic materials. A modified simulated annealing method was used for the fitting procedure (see Ref.51 for more details).

Five adjustable parameters for diamond and Si, and a total of six adjustable parameters for Ge were used to fit the calculated bandstructure to seven different experimental transition energies (which were obtained from Ref. 110). Additional constraints were imposed to ensure the correct band ordering of valence states and conduction states.

As can be seen in table.VIII, our fits are in excellent agreement with experiment. The fitting parameters for the form factors, used for obtaining the results shown in table.VIII, are given in table.IX and the atomic form factors themselves are shown in fig.6. The calculated ZB bandstructures of these group-IV semiconductors are shown in fig.7. Note that for cubic diamond and Si, the p -like conduction band states are below the s -like state. In addition, these are also indirect gap semiconductors with

diamond			Si			Ge		
Transition	Expt. (eV)	Calc. (eV)	Transition	Expt. (eV)	Calc. (eV)	Transition	Expt. (eV)	Calc. (eV)
$\Gamma_{7c}^- - \Gamma_{8v}^+$	7.3	7.3	$\Gamma_{7c}^- - \Gamma_{8v}^+$	3.35	3.35	$\Gamma_{7c}^- - \Gamma_{8v}^+$	0.898	0.898
$\Gamma_{6c}^- - \Gamma_{8v}^+$	12.9	12.854	$\Gamma_{6c}^- - \Gamma_{8v}^+$	4.15	4.148	$\Gamma_{6c}^- - \Gamma_{8v}^+$	3.22	3.223
$\Gamma_{8v}^+ - \Gamma_{6v}^+$	26	26.779	$\Gamma_{8v}^+ - \Gamma_{6v}^+$	12.5	12.707	$\Gamma_{8v}^+ - \Gamma_{6v}^+$	12.6	12.286
$L_{6c}^+ - L_{6v}^-$	10.5	10.508	$L_{6c}^+ - \Gamma_8^+$	2.05	2.072	$L_{6c}^+ - \Gamma_8^+$	0.76	0.76
$X_{5c} - X_{5v}$	12.9	12.89	$X_{5c} - \Gamma_8^+$	1.13	1.13	$X_{5c} - \Gamma_8^+$	1.16	1.081
Δ_{so}	0.006	0.006	Δ_{so}	0.441	0.441	Δ_{so}	0.297	0.297
Δ'_{so}	-	-	Δ'_{so}	-	-	Δ'_{so}	0.2	0.2

Table VIII. A comparison between targeted experimental transition energies taken from Ref.[110] and the calculated values for cubic diamond, Si and Ge. For each material, the first column shows the targeted transitions, the second column shows the targeted energies and the third column shows the converged results from fitting the pseudopotentials. The spin-orbit splitting energies are $\Delta_{so} = E_{8v}^\Gamma - E_{7v}^\Gamma$ and for Ge, $\Delta'_{so} = E_{8c}^\Gamma - E_{6c}^\Gamma$.

Material	x_1	x_2	x_3	x_4	μ_1	μ_2
diamond	444.305	-1716.53	0.0263	6.2294	12.515	-
Si	8.2808	-54.1842	0.0116	4.7922	0.0536	-
Ge	0.0791	-0.5737	0.0247	-1.2269	0.2413	8.4571e-17

Table IX. The x_j s are the fitting parameters for the form factors and spin-orbit splitting energies and μ_1 and μ_2 are the fitting parameters for the spin-orbit coupling. Note that the form factors are in units of Ry .

the conduction band minima lying in very close proximity to the X -valley along the Δ -direction.

- ¹ A. Mujica, A. Rubio, A. Muñoz, and R. J. Needs, Rev. Mod. Phys. **75**, 863 (2003).
- ² C. Frondel and U. B. Marvin, Nature **214**, 587 (1967).
- ³ F. P. Bundy and J. S. Kasper, J. Chem. Phys. **46**, 4737 (1967).
- ⁴ G. J. Ackland, Reports on Progress in Physics **64**, 483 (2001).
- ⁵ M. I. McMahon and R. J. Nelmes, Phys. Rev. Lett. **95**, 215505 (2005).
- ⁶ Y. Zhang, Z. Iqbal, S. Vijayalakshmi, and H. Grebel, Applied Physics Letters **75**, 2758 (1999).
- ⁷ M. Koguchi, H. Kakibayashi, M. Yazawa, K. Hiruma, and T. Katsuyama, Jpn. J. Appl. Phys. **31**, 2061 (1992).
- ⁸ M. Mattila, T. Hakkarainen, M. Mulot, and H. Lipsanen, Nanotechnology **17**, 1580 (2006).
- ⁹ K. Tomioka, J. Motohisa, S. Hara, and T. Fukui, Jpn. J. Appl. Phys. **46**, L1102 (2007).
- ¹⁰ T. Akiyama, K. Nakamura, and T. Ito, Phys. Rev. B **73**, 235308 (2006).
- ¹¹ M. Galicka, M. Bukala, R. Buczko, and P. Kacman, Journal of Physics: Condensed Matter **20**, 454226 (2008).
- ¹² V. G. Dubrovskii and N. V. Sibirev, Phys. Rev. B **77**, 035414 (2008).
- ¹³ F. Glas, J.-C. Harmand, and G. Patriarche, Phys. Rev. Lett. **99**, 146101 (2007).
- ¹⁴ Y. Haneda, T. Akiyama, K. Nakamura, and T. Ito, Applied Surface Science **254**, 7746 (2008), ISSN 0169-4332, 9th International Conference on Atomically Controlled Surfaces, Interfaces and Nanostructures 2007 (ASCIN-9).
- ¹⁵ J. Arbiol, A. F. i Morral, S. Estradé, F. Peiró, B. Kalache, P. R. i Cabarrocas, and J. R. Morante, Journal of Applied Physics **104**, 064312 (2008).
- ¹⁶ A. Fontcuberta i Morral, J. Arbiol, J. Prades, A. Cirera, and J. R. Morante, Advanced Materials **19**, 1347 (2007).
- ¹⁷ I. Ponomareva, M. Menon, D. Srivastava, and A. N. Andriotis, Phys. Rev. Lett. **95**, 265502 (2005).
- ¹⁸ R. Kagimura, R. W. Nunes, and H. Chacham, Phys. Rev. Lett. **95**, 115502 (2005).
- ¹⁹ D.-B. Zhang, M. Hua, and T. Dumitrică, The Journal of Chemical Physics **128**, 084104 (pages 9) (2008).
- ²⁰ X. Liu and D. Wang, Nano Research **2**, 575 (2009), ISSN 1998-0124.
- ²¹ L. Hu and G. Chen, Nano Lett. **7**, 3249 (2007).
- ²² L. Tsakalakos, J. Balch, J. Fronheiser, B. A. Korevaar, O. Sulima, and J. Rand, Appl. Phys. Lett. **91**, 233117 (pages 3) (2007).
- ²³ J. A. Czaban, D. A. Thompson, and R. R. LaPierre, Nano Lett. **9**, 148 (2009).
- ²⁴ T. Henry, K. Kim, Z. Ren, C. Yerino, J. Han, and H. X. Tang, Nano Lett. **7**, 3315 (2007).
- ²⁵ C. Balocco, A. M. Song, M. Aberg, A. Forchel, T. Gonzalez, J. Mateos, I. Maximov, M. Missous, A. A. Rezazadeh, J. Saijets, et al., Nano Lett. **5**, 1423 (2005).
- ²⁶ S. Gustavsson, I. Shorubalko, R. Leturcq, T. Ihn, K. Ensslin, and S. Schön, Phys. Rev. B **78**, 035324 (pages 7) (2008).
- ²⁷ K. M. Rosfjord, J. K. W. Yang, E. A. Dauler, A. J. Kerman, V. Anant, B. M. Voronov, G. N. Gol'tsman, and K. K. Berggren, Opt. Express **14**, 527 (2006).
- ²⁸ C. Zinoni, B. Alloing, L. H. Li, F. Marsili, A. Fiore, L. Lunghi, A. Gerardino, Y. B. Vakhtomin, K. V. Smirnov, and G. N. Gol'tsman, Appl. Phys. Lett. **91**, 031106 (pages 3) (2007).
- ²⁹ E. Dauler, B. Robinson, A. Kerman, J. Yang, E. Rosfjord, V. Anant, B. Voronov, G. Gol'tsman, and K. Berggren,

- Applied Superconductivity, IEEE Transactions on **17**, 279 (2007), ISSN 1051-8223.
- ³⁰ Y. Cui, Z. Zhong, D. Wang, W. U. Wang, and C. M. Lieber, Nano Lett. **3**, 149 (2003).
 - ³¹ A. B. Greytak, L. J. Lauhon, M. S. Gudiksen, and C. M. Lieber, Appl. Phys. Lett. **84**, 4176 (2004).
 - ³² C. Thelander, T. M. rtensson, M. T. Björk, B. J. Ohlsson, M. W. Larsson, L. R. Wallenberg, and L. Samuelson, Appl. Phys. Lett. **83**, 2052 (2003).
 - ³³ M. T. Björk, B. Ohlsson, T. Sass, A. Persson, C. Thelander, M. Magnusson, K. Deppert, L. R. Wallenberg, and L. Samuelson, Appl. Phys. Lett. **80**, 1058 (2002).
 - ³⁴ M. T. Björk, B. J. Ohlsson, C. Thelander, A. I. Persson, K. Deppert, L. R. Wallenberg, and L. Samuelson, Appl. Phys. Lett. **81**, 4458 (2002).
 - ³⁵ N. Panev, A. I. Persson, N. Sköld, and L. Samuelson, Appl. Phys. Lett. **83**, 2238 (2003).
 - ³⁶ X. Duan, Y. Huang, Y. Cui, J. Wang, and C. M. Lieber, Nature **409**, 66 (2001).
 - ³⁷ L. Samuelson, C. Thelander, M. T. Bjrk, M. Borgstrm, K. Deppert, K. A. Dick, A. E. Hansen, T. Mrtensson, N. Panev, A. I. Persson, et al., Physica E **25**, 313 (2004).
 - ³⁸ J. D. Joannopoulos and M. L. Cohen, Phys. Rev. B **7**, 2644 (1973).
 - ³⁹ M. R. Salehpour and S. Satpathy, Phys. Rev. B **41**, 3048 (1990).
 - ⁴⁰ M. Murayama and T. Nakayama, Phys. Rev. B **49**, 4710 (1994).
 - ⁴¹ C. Raffy, J. Furthmüller, and F. Bechstedt, Phys. Rev. B **66**, 075201 (2002).
 - ⁴² J. L. Birman, Phys. Rev. Lett. **2**, 157 (1959).
 - ⁴³ T. K. Bergstresser and M. L. Cohen, Phys. Rev. **164**, 1069 (1967).
 - ⁴⁴ C. P. Foley and T. L. Tansley, Phys. Rev. B **33**, 1430 (1986).
 - ⁴⁵ Z. Z. Bandić and Z. Ikonić, Phys. Rev. B **51**, 9806 (1995).
 - ⁴⁶ S. K. Pugh, D. J. Dugdale, S. Brand, and R. A. Abram, J. Appl. Phys. **86**, 3768 (1999).
 - ⁴⁷ G. Pennington and N. Goldsman, Phys. Rev. B **64**, 045104 (2001).
 - ⁴⁸ D. Fritsch, H. Schmidt, and M. Grundmann, Phys. Rev. B **67**, 235205 (2003).
 - ⁴⁹ D. Fritsch, H. Schmidt, and M. Grundmann, Appl. Phys. Lett. **88**, 134104 (2006).
 - ⁵⁰ M. Cohen and J. R. Chelikowsky, *Electronic Structure and Optical Properties of Semiconductors* (Springer, Berlin, 1988).
 - ⁵¹ A. De and C. E. Pryor, Phys. Rev. B **81**, 155210 (2010).
 - ⁵² B. V. Novikov, S. Y. Serov, N. G. Filosofov, I. V. Shtrom, V. G. Talalaev, O. F. Vyvenko, E. V. Ubyivovk, Y. B. Samsonenko, A. D. Bouravleuv, I. P. Soshnikov, et al., physica status solidi (RRL) Rapid Research Letters **4**, 175 (2010).
 - ⁵³ B. Ketterer, M. Heiss, E. Uccelli, J. Arbiol, and A. Fontcuberta i Morral, ACS Nano **5**, 7585 (2011).
 - ⁵⁴ M. Heiss, S. Conesa-Boj, J. Ren, H.-H. Tseng, A. Gali, A. Rudolph, E. Uccelli, F. Peiró, J. R. Morante, D. Schuh, et al., Phys. Rev. B **83**, 045303 (2011).
 - ⁵⁵ W. Peng, F. Jabeen, B. Jusserand, J. C. Harmand, and M. Bernard, Applied Physics Letters **100**, 073102 (pages 3) (2012).
 - ⁵⁶ U. Jahn, J. Lähnemann, C. Pfüller, O. Brandt, S. Breuer, B. Jenichen, M. Ramsteiner, L. Geelhaar, and H. Riechert, Phys. Rev. B **85**, 045323 (2012).
 - ⁵⁷ J. Wallentin, K. Mergenthaler, M. Ek, L. R. Wallenberg, L. Samuelson, K. Deppert, M.-E. Pistol, and M. T. Borgstrom, Nano Letters **11**, 2286 (2011).
 - ⁵⁸ J. Wang, M. S. Gudiksen, X. Duan, Y. Cui, and C. M. Lieber, Science **293**, 1455 (2001).
 - ⁵⁹ M. Mattila, T. Hakkarainen, H. Lipsanen, H. Jiang, and E. I. Kauppinen, Appl. Phys. Lett. **90**, 033101 (2007).
 - ⁶⁰ A. Mishra, L. V. Titova, T. B. Hoang, H. E. Jackson, L. M. Smith, J. M. Yarrison-Rice, Y. Kim, H. J. Joyce, Q. Gao, H. H. Tan, et al., Appl. Phys. Lett. **91**, 263104 (pages 3) (2007).
 - ⁶¹ A. Lan, J. Giblin, V. Protasenko, and M. Kuno, Appl. Phys. Lett. **92**, 183110 (pages 3) (2008).
 - ⁶² Y. Kobayashi, M. Fukui, J. Motohisa, and T. Fukui, Physica E: Low-dimensional Systems and Nanostructures **40**, 2204 (2008), ISSN 1386-9477, 13th International Conference on Modulated Semiconductor Structures.
 - ⁶³ D. D. D. Ma, S. T. Lee, and J. Shinar, Applied Physics Letters **87**, 033107 (pages 3) (2005).
 - ⁶⁴ J. L. Birman, Phys. Rev. **114**, 1490 (1959).
 - ⁶⁵ A. H. W. Streitwolf, Physica Status Solidi (b) **33**, 225 (1969).
 - ⁶⁶ P. Sercel and K. Vahala, Physical Review B **42**, 3690 (1990).
 - ⁶⁷ M. Cardona and G. Harbeke, Phys. Rev. **137**, A1467 (1965).
 - ⁶⁸ D. C. Reynolds, C. W. Litton, and T. C. Collins, Phys. Rev. **140**, A1726 (1965).
 - ⁶⁹ Y.-N. Xu and W. Y. Ching, Phys. Rev. B **48**, 4335 (1993).
 - ⁷⁰ S. Ninomiya and S. Adachi, Journal of Applied Physics **78**, 1183 (1995).
 - ⁷¹ T. Kawashima, H. Yoshikawa, S. Adachi, S. Fuke, and K. Ohtsuka, Journal of Applied Physics **82**, 3528 (1997).
 - ⁷² A. Alemu, B. Gil, M. Julier, and S. Nakamura, Phys. Rev. B **57**, 3761 (1998).
 - ⁷³ M. Rohlfing and S. G. Louie, Phys. Rev. Lett. **81**, 2312 (1998).
 - ⁷⁴ B. Arnaud and M. Alouani, Phys. Rev. B **63**, 085208 (2001).
 - ⁷⁵ G. Onida, L. Reining, and A. Rubio, Rev. Mod. Phys. **74**, 601 (2002).
 - ⁷⁶ R. Laskowski, N. E. Christensen, G. Santi, and C. Ambrosch-Draxl, Phys. Rev. B **72**, 035204 (2005).
 - ⁷⁷ S. Ismail-Beigi, Phys. Rev. B **77**, 035306 (2008).
 - ⁷⁸ T. Puangmali, M. Califano, and P. Harrison, Phys. Rev. B **78**, 245104 (2008).
 - ⁷⁹ B. D. Malone, S. G. Louie, and M. L. Cohen, Phys. Rev. B **81**, 115201 (2010).
 - ⁸⁰ F. Trani, G. Cantele, D. Ninno, and G. Iadonisi, Phys. Rev. B **72**, 075423 (2005).
 - ⁸¹ I. J. Wu and G. Y. Guo, Phys. Rev. B **76**, 035343 (2007).
 - ⁸² L. Makinistian, E. A. Albanesi, N. V. Gonzalez Lemus, A. G. Petukhov, D. Schmidt, E. Schubert, M. Schubert, Y. B. Losovyj, P. Galiy, and P. Dowben, Phys. Rev. B **81**, 075217 (2010).
 - ⁸³ H. Kageshima and K. Shiraishi, Phys. Rev. B **56**, 14985 (1997).
 - ⁸⁴ B. Adolph, J. Furthmüller, and F. Bechstedt, Phys. Rev. B **63**, 125108 (2001).
 - ⁸⁵ C. J. Pickard and F. Mauri, Phys. Rev. B **63**, 245101 (2001).
 - ⁸⁶ P. Monachesi, A. Marini, G. O. and M. Palummo, and R. D. Sole, physica status solidi (a) **184**, 101 (2001).

- ⁸⁷ V. I. Gavrilenko and F. Bechstedt, Phys. Rev. B **54**, 13416 (1996).
- ⁸⁸ V. I. Gavrilenko and F. Bechstedt, Phys. Rev. B **55**, 4343 (1997).
- ⁸⁹ W. G. Schmidt, S. Glutsch, P. H. Hahn, and F. Bechstedt, Phys. Rev. B **67**, 085307 (2003).
- ⁹⁰ M. S. Hybertsen and S. G. Louie, Phys. Rev. B **35**, 5585 (1987).
- ⁹¹ S. de Gironcoli, S. Baroni, and R. Resta, Phys. Rev. Lett. **62**, 2853 (1989).
- ⁹² Z. H. Levine and D. C. Allan, Phys. Rev. B **43**, 4187 (1991).
- ⁹³ H. Ehrenreich, F. Seitz, and D. Turnbull, eds., *Solid State Physics: Advances in Research and Application*, vol. 24 (Academic Press, NY and London, 1970).
- ⁹⁴ J.-B. Xia, Phys. Rev. B **38**, 8358 (1988).
- ⁹⁵ C.-Y. Yeh, S. B. Zhang, and A. Zunger, Phys. Rev. B **50**, 14405 (1994).
- ⁹⁶ W. J. Fan, J. B. Xia, P. A. Agus, S. T. Tan, S. F. Yu, and X. W. Sun, Journal of Applied Physics **99**, 013702 (pages 4) (2006).
- ⁹⁷ G. Weisz, Phys. Rev. **149**, 504 (1966).
- ⁹⁸ J. R. Chelikowsky and M. L. Cohen, Phys. Rev. B **14**, 556 (1976).
- ⁹⁹ F. Herman and S. Skillman, *Atomic Structure Calculations* (Prentice-Hall, Englewood Cliffs, N. J., 1963).
- ¹⁰⁰ M. Hendriks, S. Radelaar, A. Beers, and J. Bloem, Thin Solid Films **113**, 59 (1984), ISSN 0040-6090.
- ¹⁰¹ J. M. Besson, E. H. Mokhtari, J. Gonzalez, and G. Weill, Phys. Rev. Lett. **59**, 473 (1987).
- ¹⁰² S.-Q. Xiao and P. Pirouz, Journal of Materials Research **7**, 1406 (1992).
- ¹⁰³ M. S. Dresselhaus, G. Dresselhaus, and A. Jorio, *Group Theory: Application to the Physics of Condensed Matter* (Springer, Berlin, 2008).
- ¹⁰⁴ D. G. Thomas and J. J. Hopfield, Phys. Rev. **116**, 573 (1959).
- ¹⁰⁵ G. L. Bir and G. E. Pikus, *Symmetry and strain-induced effects in semiconductors* (Halsted, Jerusalem, 1974).
- ¹⁰⁶ C. S. Wang and B. M. Klein, Phys. Rev. B **24**, 3417 (1981).
- ¹⁰⁷ H. J. Monkhorst and J. D. Pack, Phys. Rev. B **13**, 5188 (1976).
- ¹⁰⁸ A. J. Read and R. J. Needs, Phys. Rev. B **44**, 13071 (1991).
- ¹⁰⁹ B. Adolph, V. I. Gavrilenko, K. Tenelsen, F. Bechstedt, and R. Del Sole, Phys. Rev. B **53**, 9797 (1996).
- ¹¹⁰ O. Madelung, ed., *Semiconductors Data Handbook* (Springer-Verlag, Berlin Heidelberg New York, 2004), 3rd ed.
- ¹¹¹ S. L. Adler, Phys. Rev. **126**, 413 (1962).
- ¹¹² N. Wiser, Phys. Rev. **129**, 62 (1963).
- ¹¹³ M. A. Mojumder, Solid State Communications **43**, 13 (1982), ISSN 0038-1098.
- ¹¹⁴ L. R. Saravia and D. Brust, Phys. Rev. **170**, 683 (1968).